Optics Communications 380 (2016) 352–356

Contents lists available at ScienceDirect

Optics Communications

journal homepage: www.elsevier.com/locate/optcom

Groove-shape-induced bandwidth expansion of spoof surface plasmon polaritons on planar corrugated Goubau line in millimeter-wave range

Peng Wei [a], XuGuang Guo [a,b,*,1], Cheng Zhang [c], Rui Yang [c], YiMing Zhu [a,**,1]

[a] Engineering Research Center of Optical Instrument and System, Ministry of Education and Shanghai Key Lab of Modern Optical System, University of shanghai for Science and Technology, Shanghai 200093, China
[b] Key Laboratory of Terahertz Solid-State Technology, Shanghai Institute of Microsystem and Information Technology, Chinese Academy of Sciences, 865 Changning Road, Shanghai 200050, China
[c] BOCOM Smart Network Technologies Inc., 20F, Guangqi Mansion, No. 456, Hongcao Road, Xuhui District, Shanghai 200030, China

ARTICLE INFO

Article history:
Received 28 February 2016
Received in revised form
5 June 2016
Accepted 14 June 2016
Available online 21 June 2016

Keywords:
Metamaterials
Goubau line
Spoof surface plasmon polaritons

ABSTRACT

Surface plasmon polaritons (SPPs) do not exist naturally in millimeter-wave range, but can be assisted by plasmonic meta-materials, generally periodic corrugated Goubau lines (PCGLs) coated on ultrathin flexible dielectric films. Compared to traditional PCGLs with rectangular groove, we present two single-edge PCGLs with different corrugation groove shapes of triangle and trapezoid to realize more broadband transmission of spoof SPPs (SSPPs). Both the simulated and experimental results show that the pass-band of SSPPs is expanded for the PCGLs with trapezoidal and triangular grooves in the same actual depth and conversion efficiency, compared to the case of traditional rectangular grooves. The dispersion relation and the equivalent circuit model of the three SSPPs are investigated to explain the groove-shape-induced bandwidth expansion effect. The bandwidth expansion effect opens up another path to control the pass-band of SSPPs.

1. Introduction

Surface plasmon polaritons (SPPs) are propagating surface modes along the interfaces between metals and dielectrics in visible and near-infrared regions [1]. Owning to their extraordinary ability to confine light in a sub-wavelength scale with high intensity, SPPs attracted much attention during the last decade [2–4]. However, in microwave and terahertz regions, due to the large negative dielectric constants of metals, the dispersion relation of SPPs is similar to that of light in vacuum and traditional dielectrics [5]. Therefore, the SPPs cannot be tightly confined to the metal surfaces, and they also cannot travel a long distance along the metal surfaces because of large radiation loss.

Plasmonic materials, generally formed by drilled metal surfaces with periodical sub-wavelength holes and other structures have been proposed to make SPPs in millimeter wave frequency come true, which are called spoof SPPs (SSPPs) [6–8]. Early investigation of SSPPs stems from the study of a single metal wire transmission line used to conduct radio waves in ultrahigh frequency and microwave frequency by Goubau in 1950s [9]. But the absence of efficient conversion section for phase-matching between the electromagnetic waves and the SSPPs restricts applications of SSPPs in microwave and terahertz regions. Recently, SSPPs propagating along planar corrugated Goubau lines (PCGLs) deposited on ultrathin and flexible substrates have been proposed and demonstrated [10]. A tapered coplanar waveguide (CPW) structure [11] is used to convert the quasi transverse electric and magnetic wave (QTEM) guided by a CPW into SSPPs propagating along the PCGL with high efficiency. Such planar CPW-PCGL structures have advantages in integration and make it convenient to apply SSPPs to the applications of super-resolution imaging [12], electromagnetically induced transparency (EIT) [13,14], environmental detection, and bio-sensing [15,16]. At the present stage, many related investigations on the CPW-PCGL structures have been concentrated on coupling efficiency, bandwidth, transmission loss, and the enhancement of local electromagnetic field [17–25]. The bandwidth of SSPPs on the ultrathin PCGLs is increased significantly by reducing the depth of corrugation grooves. However, such design approach does not only alter the bandwidth, but also change the phase-matching condition between the CPW component and the PCGL component. Therefore, it brings low coupling

* Corresponding author at: Engineering Research Center of Optical Instrument and System, Ministry of Education and Shanghai Key Lab of Modern Optical System, University of shanghai for Science and Technology, Shanghai 200093, China.
** Corresponding author.
E-mail addresses: xgguo@mail.sim.ac.cn (X. Guo), ymzhu@usst.edu.cn (Y. Zhu).
[1] Equal contribution.

http://dx.doi.org/10.1016/j.optcom.2016.06.038
0030-4018/

efficiency to increase the depth of the corrugation grooves simply in traditional method. And this method is also difficult to design accurate fabrication. Meanwhile, it is important to systematically explore the effects of structural parameters on the transmission performance of CPW-PCGLs. Compared to the traditional CPW-PCGLs by changing the whole structure, we transform the shape of PCGLs' groove to get smaller equivalent groove depth. This method realizes higher cut-off frequency while the actual groove depth is not changed. Moreover, CPW-PCGLs can reach broadband transmission with high coupling efficiency and be easily fabricated simultaneously in this way.

In this work, three single-edge PCGLs with different corrugation groove shapes of triangle, trapezoid, and rectangle have been meticulously designed, fabricated, and measured from 15 GHz to 75 GHz. As traditional method, the rectangle is the sample for comparison with the other two. The simulated results and experimental data of transmission coefficients of the three PCGLs are in good accordance with each other. The structures with rectangular, trapezoidal, and triangular grooves have cut-off frequency of 49.01 GHz, 53.33 GHz, and 63.23 GHz, respectively. The groove-shape-induced bandwidth expansion effect of SSPPs is clearly observed. The bandwidth of the CPW-PCGL with trapezoidal and triangular grooves is improved by about 8% and 26% respectively in the same actual depth and conversion efficiency, compared to that of the CPW-PCGL with rectangular grooves. Moreover, both simulated and measured S-parameters show that different corrugation groove shapes have little influence on transmission coefficients in the pass-band and just affect the cut-off frequencies of SSPPs. It can be widely used to increase the bandwidth without changing the CPW and the tapered CPW structural parameters and play a significant role in CPW-PCGLs of limit strip width. This effect will open up another path to control bandwidth of SSPPs for the CPW-PCGL structures and this method can be generalized to other frequency, such as Terahertz.

2. CPW-PCGL structure design

Fig. 1 shows the schematics of the hybrid CPW-PCGL structure. The 50-Ω CPW section with $H=0.15$ mm and $s=0.01$ mm is a convenient interface for measurement and constructing application systems. The tapered CPW section II is used to reduce the mismatch between 50-Ω CPW and high impedance PCGL. It has been well approved that such tapered CPW structure can effectively couple the QTEM modes into SSPPs. Based on the scheme proposed by Ma et al. [11], the symmetric profile of the tapered CPW is described by the following analytical expression:

$$y = C_1 e^{\alpha \cdot x} + C_2,\ C_1 = \frac{y_2 - y_1}{e^{\alpha x_2} - e^{\alpha x_1}},\ C_2 = \frac{y_2 e^{(\alpha x_1)} - y_1 e^{(\alpha x_2)}}{e^{(\alpha x_2)} - e^{(\alpha x_1)}} \quad (1)$$

Where α is free parameter, (x_1, y_1) and (x_2, y_2) are the coordinates of the starting and ending points of the exponential slot line.

At the same time, the depths of corrugation grooves in the transition increase from $h_1=0.125$ mm to $h_8=1$ mm with a step of 0.125 mm. A commercial software CST Microwave Studio is used to optimize the tapered CPW structure. The optimized values of parameters α, x_2–x_1, y_2–y_1 are 2, 2.8 mm, and 2.5 mm, respectively. The highest designed cut-off frequency of the CPW-PCGL is about 70 GHz. For higher cut-off frequency, the effects of dielectric loss and the metal loss due to the imperfection of metal strips become significant, which has negative influence on the investigation of bandwidth expansion effect induced by corrugation groove shape.

We select 215-μm-thick flexible polyethylene naphthalate [24] (PEN) as substrate to reduce loss of dielectric material. Three designed CPW-PCGL structures with different corrugation groove shapes were fabricated using optical lithography and wet-chemical etching techniques. The metal strips are composed of Ti (50 nm)/Au (300 nm) films.

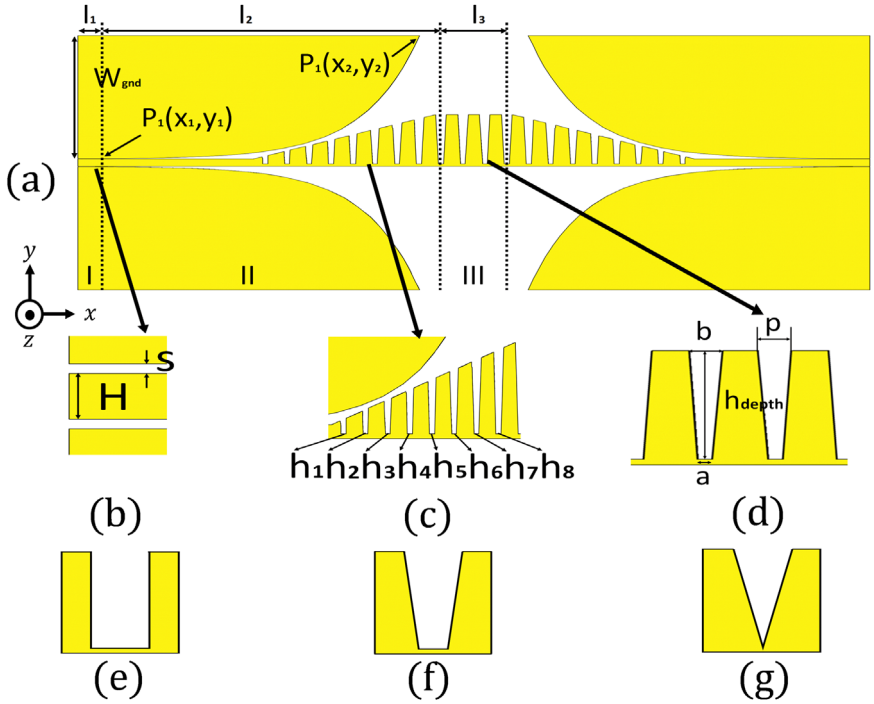

Fig. 1. (a) Schematic of the CPW-PCGL structure with $l_1=0.1$ mm, $l_2=3$ mm, $l_3=0.6$ mm, and $W_{gnd}=2.5$ mm; (b) CPW section with $H=0.15$ mm and $s=0.01$ mm; (c) Tapered CPW section. The depths of groves linearly increase from $h_1=0.125$ mm to $h_8=1$ mm with a step of 0.125 mm; (d) Corrugation grove parameters $b=0.1$ mm, $p=0.2$ mm, and $h_{depth}=h_8$; (e)-(g) Groove shapes of rectangle, trapezoid, and triangle with $a=0.1$ mm, 0.05 mm, and 0 mm, respectively.

3. S-parameters and discussion

To demonstrate the bandwidth expansion effect induced by the groove shape quantitatively, the S_{21} and S_{11} parameters as shown in Fig. 2 are measured by using a vector network analyzer (VNA) for the frequency from 15 GHz to 75 GHz. We can notice that the transmission coefficients S_{21} are about -5 dB in the whole pass-band for the three cases, while insertion losses S_{11} are below -10 dB in a wide frequency range of 15–50 GHz. The excellent transmission indicates high coupling efficiency between the CPW section and the PCGL section. There are three factors to guarantee such high coupling efficiencies. First, the tapered ground planes could efficiently transform QTEM modes supported by the CPW into Goubau modes propagating in the metallic strip since the electric energy radiated by the Vivaldi slot has a spherical-like wave front [26]. Secondly, the graded depth of grooves of PCGL in the tapered CPW transition could soften the wave vector mismatch between radiated electromagnetic waves and SSPPs. Finally, the electric fields could be adapted vertical to metallic strips by beveled grooves. The tapered ground planes and the graded depth of groves could effectively avoid extra radiation loss coming out of Vivaldi slot and reflection by impedance mismatch. Meanwhile, the measurement results show that the coupling efficiency is not affected by the corrugation groove shape. The measured S_{11} parameters are lower than the simulated ones in the pass-band, which means that section II has better conversion efficiency than we expected and the whole structure manifests lower mismatching tolerance and metallic loss. Imperfect fabrication of structures results in little disturbance in the pass-band frequency.

The groove-shape-induced pass-band expansion effect is also clearly exhibited by the measured S_{21} parameters as shown in Fig. 2. The simulated S-parameters of different groove shapes by CST microwave studio software shown by dotted line in Fig. 2 are in good accordance with the measurement results, which further identifies that the bandwidth expansion originates from the corrugation groove shape. The CPW-PCGL structures with rectangular, trapezoidal, and triangular grooves have cut-off frequency of 49.01 GHz, 53.33 GHz, and 63.23 GHz, respectively. It means that the pass-band of SSPPs expands 8% and 26% for the PCGLs with trapezoidal and triangular grooves in the same actual depth and conversion efficiency, compared to the case of traditional rectangular grooves. Moreover, comparing *S*-parameters of different structures, we note that the groove shape has little impact on transmission coefficient of pass-band and only affects cut-off frequency of SSPPs.

4. Theory analysis of dispersion and equivalent topology

By assuming that the corrugated metal strips are infinite (It is a reasonable assumption for $l_2+l_3 \gg p$), we analyze the evolution of the dispersion relation of the three different structures by Eigenmode simulation with the CST Microwave Studio Software. As shown in Fig. 3, the cut-off frequency of the three structures is all consistent with the simulated and measured S-parameters. The saturation trends of frequency with increasing wave vector in the dispersion relation curves indicate high impendence mismatch, low group velocity, tight confinement of field, and large metallic and dielectric losses. All these factors determine the high cut-off frequency.

Moreover, we also notice that the groove shape can tailor the dispersion relation of SSPP modes. The results shown in Fig. 3 imply that the trapezoidal and triangular grooves provide weaker EM confinement compared to rectangular grooves at the same frequency. However, it has been well confirmed that there is a trade-off between the bandwidth and the EM confinement in low frequency region for the PCGL structures. Such side effect is not only introduced by the change of groove shape, but also an intrinsic property of the PCGL structures, as shown by Ma et al. [11].

To confirm the side effect, insertion in Fig. 3 shows slowdown factor *S* for the SSPP modes guided by the rectangular, trapezoidal, and triangular grooves. Perturbation near cutoff frequency is due to simulation accuracy error by CST.

To describe the EM confinement and enhancement, the slowdown factor $S=V_g/V_p$ is introduced, where V_g and V_p are the group and phase velocities, respectively. The slowdown factor *S* is the measurement of the confinement and enhancement of EM fields. The maximum value of $S=1.0$ implies no EM confinement and enhancement effects, and a smaller value of *S* means stronger EM confinement. The insertion of Fig. 3 shows the slowdown factor *S* for the SSPP modes guided by the rectangular, trapezoidal, and triangular grooves.

We could find that the values of slowdown factor *S* for the three structures are all greater than 0.8 below 30 GHz, which means that the EM confinement of the three structures is weak in the frequency range of 15–30 GHz. In higher frequency region, the differences of the slowdown factors among the three structures increase. As shown in Fig. 2 and Fig. 3, the values of the slowdown factor *S* for the three structures are all below 0.1 at the cut-off frequencies of 49.01, 53.33, and 63.23 GHz, respectively. Therefore, we could conclude that the trapezoidal and triangular groove structures provide the same EM confinement ability at higher frequencies compared to the rectangular structure. Because the groove depth and the matching condition from the CPW mode to

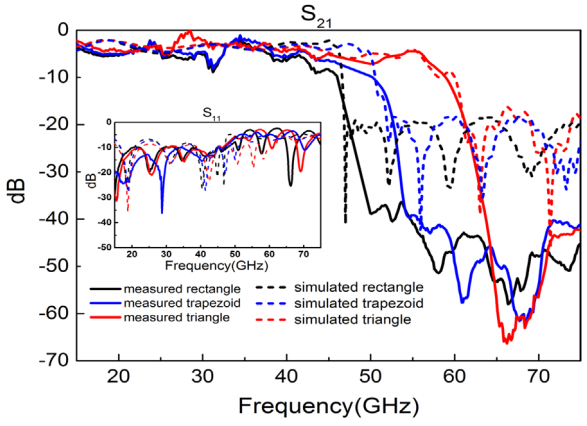

Fig. 2. Simulated and measured S21 and S11 parameters (insertion) of the hybrid CPW-PCGLs with rectangular, trapezoidal, and triangular corrugation grooves.

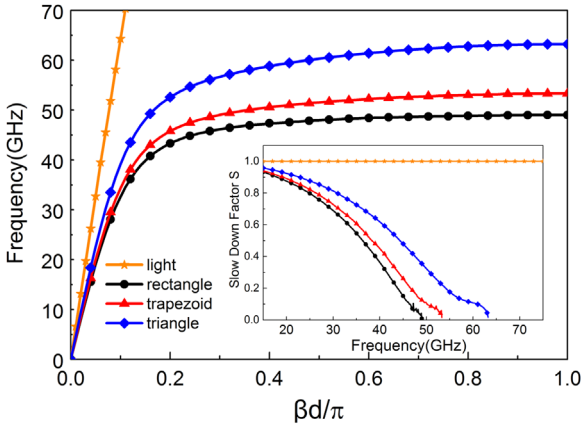

Fig. 3. Dispersion relation of PCGLs and slowdown factor S (insertion) with rectangular, trapezoidal, rectangular grooves and the light line in vacuum respectively.

the SSPP mode are not changed for the three groove structures as shown in Fig. 2, it is very convenient to design PCGL structures as sensing devices working in different frequency regions by changing the groove shapes, especially in the case of the decrease of inner section width of corrugation Goubau line being limited.

To further discuss the effect of corrugation groove shape on the high cut-off frequency, the numerical dispersion relation is fitted by constructing equivalent circuit network of the PCGL structures.

As shown in Fig. 4(a), a microwave network with periodic topology is adopted as the effective circuit model of the PCGLs. Z_0 is the characteristic impedance of Goubau line with no groove, k is the propagation constant, and d is the length of transmission line in each unit element that is p-a in this condition. Voltage and current on both sides of N_{th} unit cell (V_n, I_n, V_{n+1}, I_{n+1}) can be connected by ABCD transmission matrix.

$$\begin{bmatrix} V_n \\ I_n \end{bmatrix} = \begin{bmatrix} A & B \\ C & D \end{bmatrix} \begin{bmatrix} V_{n+1} \\ I_{n+1} \end{bmatrix} \tag{2}$$

Where A, B, C, and D are the parameters of the concatenation matrix.

The normalized matrix of a unit cell is

$$\begin{bmatrix} A & B \\ C & D \end{bmatrix} = \begin{bmatrix} \cos\frac{\theta}{2} & j\sin\frac{\theta}{2} \\ j\sin\frac{\theta}{2} & \cos\frac{\theta}{2} \end{bmatrix} \begin{bmatrix} 1 & 0 \\ jb & 0 \end{bmatrix} \begin{bmatrix} \cos\frac{\theta}{2} & j\sin\frac{\theta}{2} \\ j\sin\frac{\theta}{2} & \cos\frac{\theta}{2} \end{bmatrix}$$
$$= \begin{bmatrix} \cos\theta - \frac{b}{2}\sin\theta & j(\sin\theta + \frac{b}{2}\cos\theta - \frac{b}{2}) \\ j(\sin\theta + \frac{b}{2}\cos\theta + \frac{b}{2}) & \cos\theta - \frac{b}{2}\sin\theta \end{bmatrix} \tag{3}$$

Where $\theta = kd$. According to reciprocal network,

$$AD - BC = 1 \tag{4}$$

Assuming transmission coefficient,

$$\gamma = \alpha + i\beta \tag{5}$$

We could get relationship of βd, θ and d for the pass-band frequency.

$$\cos\beta d = \cos\theta - \frac{b}{2}\sin\theta \tag{6}$$

By fitting the numerical dispersion relation curves, the parameter b is derived for every values of βd and θ. Since the PCGLs perform as low pass filters, we could infer that b behaves as capacitive reactance. We could get distributed capacitance (scatter) as shown in Fig. 4(b). We notice that in the pass-band frequency of each structure, capacitance increases with frequency in a small range while it mounts up sharply near cut-off frequency. We notice that groove shapes have little impact on capacitance of pass-band and just keep it stable in different frequency. Corner cut of rectangle makes SSPPs in higher frequency fall into lighter depth of grooves and express lower capacitance in topology. The larger degrees corner cut is, the smaller capacitance it could be expressed in larger frequency range. As smaller capacitance leads to smaller b (larger reactance), I_{n+1} becomes larger. On the premise $V_n = V_{n+1}$, there are more power flowing past structure in higher frequency and it expresses as bandwidth expansion for the corrugation groove shapes of trapezoid and triangle.

We use MATLAB curve fitting tool to fit the relation of capacitance and frequency with the expression in Fig. 4(b) (solid green line):

$$C = a_1 \cdot e^{b_1 \cdot f} + c_1 \cdot e^{d_1 \cdot f} \tag{7}$$

Where a_1, b_1, c_1, and d_1 are fitting parameters, C is capacitance, and f is frequency. The fitting parameters of the three structures are displayed in Table 1. The fitting formula could offer reference in circuit design and simulation of the PCGLs.

To confirm effect of different shapes on transmission, we simulated the near-field distributions of E_z components for such three structures by using CST software, as illustrated in Fig. 5. In the CPW section, we observe that there are small E_z components as electric-field vectors are mainly along y-axis direction in the two ends of plasmonic waveguide. Along the matching transition section, QTEM modes supported by CPW are gradually transformed to SSPPs (or vice versa), thence the near-fields of E_z increase (or decrease) gradually. In the metallic groove strip section, plasmonic is concentrated in the grooves hence the density of E_z fields is the most intensive. Meanwhile, we verify that bounding ability at the comb side is better than the other side of metallic strip again, as Laurette showed before [27]. Comparing Fig. 5 (a)–(c), we observe that shape has little effect on coupling efficiency at

Table 1.
Distribution capacitance fitting parameters.

Shape parameters	Rectangle	Trapezoid	Triangle
a_1	3.1	3.202	3.3
b_1	0.02734	0.01968	0.001976
c_1	8.655e-13	6.42e-8	4.554e-5
d_1	0.6633	0.3966	0.2259

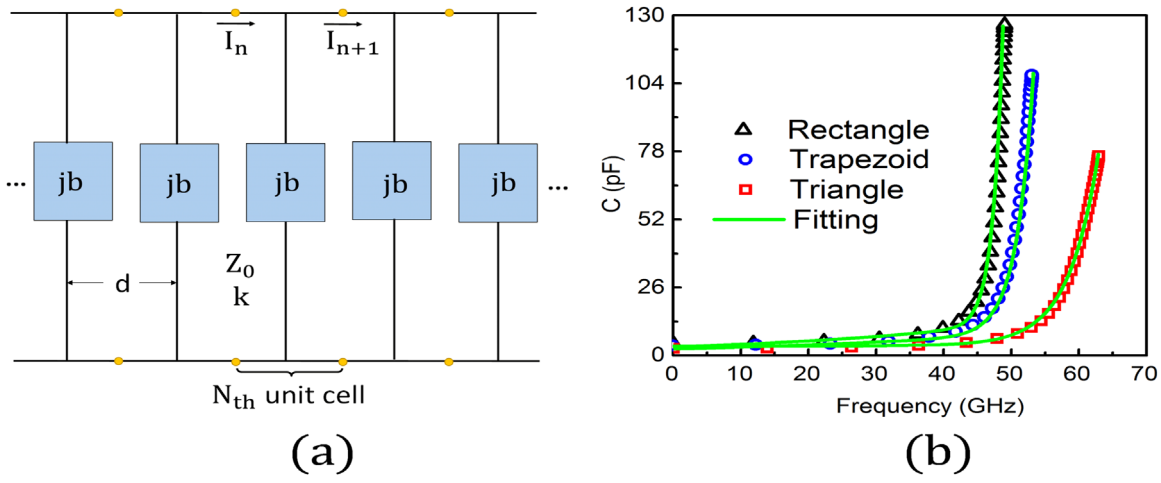

Fig. 4. (a) The effective network model of the periodic PCGL structure; (b) The fitting values of frequency-dependent capacities of the three groove shapes within a periodic microwave network model.

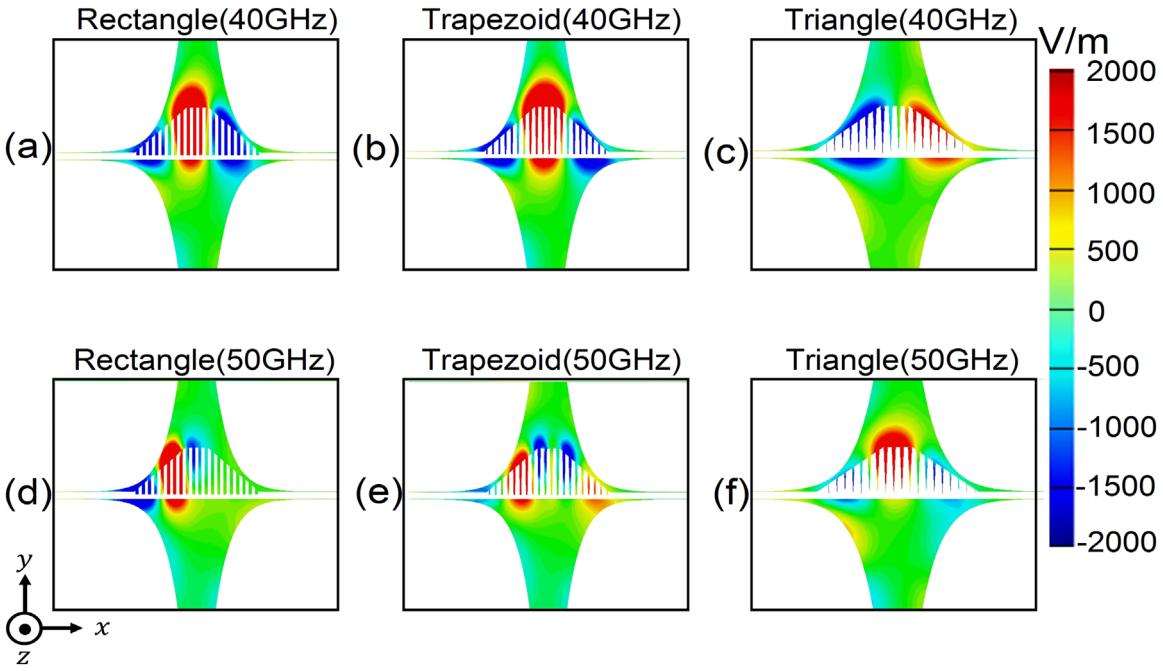

Fig.5. Three shape grooves near-field distributions of E_z components at 40 GHz and 50 GHz, respectively.

band pass frequency (40 GHz) and smaller effective depth has larger wavelength corresponding to triangle, trapezoid, and rectangle from the smallest one to the largest one. At 50 GHz, SSPPs could not flow through rectangle groove structure because of its groove depth in Fig. 5(d) and trapezoid is disturbed as it is close to cut-off frequency in Fig. 5(e). Shown by Fig. 5(f), we notice that SSPPs could go through the structure normally. Comparing pictures in Fig. 5, we could note that shape only affect cut-off frequency and has little influence on near electric-field distributions in pass-band.

5. Conclusion

We have presented two single-edge PCGLs with different corrugation groove shapes of triangle and trapezoid to verify bandwidth expansion effect of SSPPs in contrast with traditional rectangle. Both the simulated and experimental S-parameters show that the pass-band of SSPPs expands 8% and 26% for the PCGLs with trapezoidal and triangular grooves respectively. We broaden bandwidth in the same actual depth and conversion efficiency, compared to the case of traditional rectangular grooves. Then we analyze the dispersion and equivalent Circuit topology of PCGLs, and they are consistent with simulated and measured S-parameters. And near-field distributions E_z of SSPPs in the grooves show that difference of groove shapes has little influence on pass-band transmission.

Owing to such bandwidth expansion effect, it is possible to realize higher bandwidth, more excellent transmission, more convenient planar advanced plasmonic functional device and integrated circuits without changing depth of the corrugation groove, which has significant influence on the bandwidth of SSPPs on ultrathin PCGLs. This effect opens up another path to control bandwidth of SSPPs for CPW-PCGL structures.

Acknowledgments

This work was partly supported by the National Program on Key Basic Research Project of China (973 Program, 2014CB339806), Basic Research Key Project (12JC1407100), Major National Development Project of Scientific Instrument and Equipment (2011YQ150021) (2012YQ14000504), National Natural Science Foundation of China (11174207) (61138001) (61205094) (61307126), Program of Shanghai Subject Chief Scientist (14XD1403000), Project Supported by Shanghai Municipal Science and Technology Commission (14dz1206600), and the New Century Excellent Talents Project from the Ministry of Education (NCET-12–1052).

References

[1] W.L. Barnes, A. Dereux, T.W. Ebbesen, Nature 424 (2003) 6950.
[2] F.R. Yang, K.P. Ma, Y. Qian, T. Itoh, IEEE Trans. Microw. Theory Tech. 47 (1999) 8.
[3] D.J. Blumenthal, P.R. Prucnal, J.R. Sauer, Proc. IEEE 82 (1994) 11.
[4] E.N. Economou, Phys. Rev. 182 (1969) 2.
[5] F.J. Garcia-Vidal, L. Martin-Moreno, J.B. Pendry, J. Opt. A: Pure Appl. Opt. 7 (2005) S97.
[6] J. Zhang, L. Cai, W. Bai, Y. Xu, G. Song, J. Appl. Phys. 106 (2009) 103715.
[7] A.P. Hibbins, B.R. Evans, J.R. Sambles, Sci. 308 (2005) 5722.
[8] D. Martin-Cano, M.L. Nesterov, A.I. Fernandez-Dominguez, F.J. Garcia-Vidal, L. Martin-Moreno, E. Moreno, Opt. Express 18 (2010) 2.
[9] G. Goubau, J. Appl. Phys. 21 (1950) 11.
[10] X. Shen, T.J. Cui, D. Martin-Cano, F.J. Garcia-Vidal, PNAS 110 (2013) 1.
[11] H.F. Ma, X. Shen, Q. Cheng, W.X. Jiang, T.J. Cui, Laser Photonics Rev. 8 (2014) 1.
[12] D. Lu, Z. Liu, Nat. Commun. 3 (2012).
[13] Z. Han, S.I. Bozhevolnyi, Opt. Express 19 (2011) 4.
[14] L. Chen, C.M. Gao, J.M. Xu, X.F. Zang, B. Cai, Y.M. Zhu, Opt. Lett. 38 (2013) 1379.
[15] A.V. Kabashin, P. Evans, S. Pastkovsky, W. Hendren, G.A. Wurtz, R. Atkinson, A. V. Zayats, Nat. Mater. 8 (2009) 11.
[16] D.R. Chowdhury, N. Xu, W. Zhang, R. Singh, J. Appl. Phys. 118 (2015) 2.
[17] S.I. Bozhevolnyi, V.S. Volkov, E. Devaux, J.Y. Laluet, T.W. Ebbesen, Nature 440 (2006) 7083.
[18] M. Ozaki, J.I. Kato, S. Kawata, Science 332 (2011) 6026.
[19] S. Sun, Q. He, S. Xiao, Q. Xu, X. Li, L. Zhou, Nat. Mater. 11 (2012) 5.
[20] W.C. Chen, J.J. Mock, D.R. Smith, T. Akalin, W.J. Padilla, Phy. Rev. X 1 (2011) 2.
[21] X. Shen, T.J. Cui, Appl. Phys. Lett. 102 (2013) 21.
[22] Z. Liao, J. Zhao, B.C. Pan, X.P. Shen, T.J. Cui, J. Phys. D: Appl. Phys. 47 (2014) 31.
[23] L. Chen, Y.M. Zhu, X.F. Zang, B. Cai, Z. Li, L. Xie, S.L. Zhuang, Light. Sci. Appl. 2 (2013) 60.
[24] D. Wang, Y. Gu, Y. Gong, C.W. Qiu, M. Hong, Opt. Express 23 (2015) 9.
[25] H.T. Chen, Opt. Express 20 (2012) 7.
[26] B.C. Pan, Z. Liao, J. Zhao, T.J. Cui, Opt. Express 22 (2014) 11.
[27] S. Laurette, A. Treizebre, B. Bocquet, IEEE Trans. Terahertz Sci. Technol. 2 (2012) 3.